Astronomy & Astrophysics manuscript no. ms˙v26
November 28, 2012

The Effects of Orbital Environment on X-ray CCD Performance

Catherine E. Grant, Beverly LaMarr, Eric D. Miller, and Marshall W. Bautz

Kavli Institute for Astrophysics and Space Research, Massachusetts Institute of Technology, Cambridge, MA 02139, USA e-mail: cgrant@space.mit.edu

ABSTRACT

Context. The performance of CCD detectors aboard orbiting X-ray observatories slowly degrades due to accumulating radiation damage.
Aims. In an effort to understand the relationship between CCD spectral resolution, radiation damage, and the on-orbit particle background, we attempt to identify differences arising in the performance of two CCD-based instruments: the Advanced CCD Imaging Spectrometer (ACIS) aboard the Chandra X-ray Observatory, and the X-ray Imaging Spectrometer (XIS) aboard the Suzaku X-ray Observatory.
Methods. We compare the performance evolution of front- and back-illuminated CCDs with one another and with that of very similar detectors installed in the ACIS instrument aboard *Chandra*, which is in a much higher orbit than *Suzaku*. We identify effects of the differing radiation environments as well as those arising from structural differences between the two types of detector.
Results. There are some differences and these are they. **don't forget to fill this in when everything else is done!**

Key words. some keywords

1. Introduction

Charged-coupled devices (CCDs) as astronomical X-ray detectors have become nearly ubiquitous since their their first use in sounding rocket flights in the late 1980s. CCDs provide excellent quantum efficiency with moderate spectral resolution over a broad energy range (∼0.1–10 keV) and are well-suited as imaging spectrometers as well as readout detectors for dispersive gratings. Currently, CCDs are focal plane detectors in five operating X-ray observatories from NASA, ESA and JAXA, and are planned to be part of many upcoming missions.

Radiation damage is a common concern in all spacecraft components. One symptom of radiation damage in CCDs is an increase in the number of charge traps (**?**) **Ref TBA**. When charge is transfered across the CCD to the readout, some portion can be captured by the traps and gradually re-emitted. If the original charge packet has been transfered away before the traps re-emit, the captured charge is "lost" to the charge packet. This process is quantified as charge transfer inefficiency (CTI), the fractional charge loss per pixel. As a result, the amount of charge (or the pulseheight) read out from the instrument decreases with increasing transfer distance; since this pulseheight corresponds directly to the incoming X-ray photon energy, the measured energy also decreases. In addition, the spectral resolution degrades due to noise in the charge trapping and re-emission process, non-uniform trap distribution, and variations in trap occupancy. All of these processes apply to the charge in each pixel, so multi-pixel X-ray events will be more degraded than single-pixel events.

Measured CTI is a function of fluence, or, more specifically, the amount of charge deposited on the CCD. As the fluence increases, traps filled by one charge packet may remain filled as a second charge packet is transferred through the pixel. The second charge packet sees fewer unoccupied traps as a result of the previous "sacrificial charge" and loses less charge than it would have otherwise (Gendreau et al. 1993). This sacrificial charge can be in the form of X-rays, charged particle interactions, or intentionally injected charge.

The response of a CCD-based instrument is thus partially determined by its particle environment, whether causing radiation damage or providing sacrificial charge, which in turn is dependent on the spacecraft orbit. The Advanced CCD Imaging Spectrometer (ACIS) on the *Chandra X-ray Observatory* (Weisskopf et al. 2002) and the X-ray Imaging Spectrometer (XIS) on the *Suzaku X-ray Observatory* (Mitsuda et al. 2007) utilize similar CCDs but occupy very different radiation environments. The two instruments combined have produced more than eighteen years worth of monitoring data which provides a unique opportunity to better understand the relationship between X-ray CCD spectral resolution, radiation damage, and the on-orbit particle background.

We begin by describing the differences and similarities of the instruments, spacecraft orbits, and on-board calibration sources in Section 2. Section 3 outlines our data analysis procedures while Section 4 discusses the results. The data used in this paper have been minimally processed and have not undergone standard pipeline processing which applies corrections to provide the best performance possible. The results here do not reflect what a typical user would find using standard data products.

2. Description of the Instruments

2.1. CCD Detector Characteristics

The CCD chips in ACIS and the XIS were fabricated at MIT Lincoln Laboratory and are very similar in design. The ACIS CCDs predate the XIS CCDs by nearly a decade so some differences do exist.

Chandra has a single X-ray telescope and a moveable Science Instrument Module (SIM), which can move ACIS in and out of the telescope focus. The ACIS focal plane consists of ten CCD devices (MIT Lincoln Laboratory CCID17), eight of which

are front-illuminated (FI) and two of which are back-illuminated (BI). The layout of the ACIS devices is shown in Figure 1. The CCD characteristics are summarized in Table 1 and described in detail by Garmire et al. (2003).

Suzaku has four XIS instruments, each with an independent X-ray Telescope (XRT) and focal plane assembly. The four devices are model CCID41, comprising three FI chips (XIS0, XIS2, and XIS3) and one BI (XIS1). The layout of the XIS devices is shown in Figure 2. One of the FI devices (XIS2) was damaged by a likely micrometorite strike in October 2006 and has been unused since that time. The characteristics of the CCDs are summarized in Table 1 and described in detail by Koyama et al. (2007). The XIS devices are physically very similar to the ACIS devices with one notable exception, the addition of charge injection capabilities in the XIS CCID41 (Bautz et al. 2007). This allows a controlled amount of charge to be injected from a register at the top of the array into individual pixels, rows, or a variety of patterns as the CCD is clocked. The injected charge is transfered along with the other charge packets in the array.

While the CCDs are reasonably similar, there are a number of important operational differences. The individual frame exposure time for XIS is more than twice as long as for ACIS. Given the same particle or X-ray flux, the longer frame time of XIS will yield more sacrificial charge than seen on ACIS. Another important difference is the operating temperature of the detector. ACIS is kept much colder than XIS (-120°C versus -90°C), which reduces the incidence of warm pixels. Depending on the characteristics of the electron traps, the temperature can also change the measured CTI. In the case of the ACIS BI CCDs, the initial CTI is all due to damage during manufacturing, and the performance is slightly better at warmer temperatures. The CTI of the ACIS FI CCDs is entirely due to radiation damage, so the CCDs are highly sensitive to temperaure and have much lower CTI at -120°C (Grant et al. 2006). Similarly, the row-to-row transfer times are slightly different which, depending on the time constants of the electron traps, can change the measured CTI.

Finally, charge injection, while initially turned off for the XIS detectors, has been the standard operating mode since November 2006 (Uchiyama et al. 2009). In this mode a full row of charge equivalent to 6 keV for the FI chips (2 keV for the BI chip) is injected every 54 rows, or every 1.3 ms during the chip read out. The level of injected charge was increased to 6 keV for the BI chip in June 2011, however we exclude those observations from the analysis presented here.

As already noted above, between the time that ACIS and XIS were built, some improvements were made in the BI manufacturing process. The ACIS BI CCDs had measurable CTI across the entire array, including the framestore and serial readout array, from defects induced in during the manufacturing process. The performance of the XIS BI CCD was nearly the same as the FI CCDs pre-launch, due to an improved thinning process further described in Burke et al. (2004) and Bautz et al. (2004).

For the purposes of this paper, we are only examining parallel CTI, or charge loss as a function of row number. Serial CTI, charge loss as a function of columns, is negligible for both XIS and ACIS except in the case of the ACIS BI CCDs, and even then it is not evolving on orbit.

2.2. Orbital Radiation Environments

ACIS and XIS occupy quite different radiation environments. *Chandra* is in a highly elliptical, 2.7-day orbit that transits a wide range of particle environments, from the Earth's radiation belts at closest approach through the magnetosphere and magnetopause and past the bow shock into the solar wind (O'Dell et al. 2000). Soon after launch it was discovered that the FI CCDs had suffered radiation damage from exposure to soft protons (~0.1–0.5 MeV) scattered off *Chandra's* grazing-incidence optics during passages through the radiation belts (Prigozhin et al. 2000). The BI CCDs were unaffected due to the much deeper buried channel. Since the discovery of the radiation damage, ACIS has been protected during radiation belt passages by moving it out of the focal plane. Radiation damage to the CCDs has continued at a much slower rate, due to soft protons scattered by the optics during observations, and strongly penetrating solar protons and cosmic rays which pass through the spacecraft shielding. The particle background on the detector consists of a quiescent portion that is anti-correlated with the solar cycle, and soft proton flares (Grant et al. 2002).

Suzaku is in a 96-minute, low-Earth orbit with an inclination of 32 degrees and gains some protection from cosmic rays by the Earth's geomagnetic field (Mitsuda et al. 2007). Many orbits pass through the South Atlantic Anomaly (SAA), a region of enhanced particle flux, which requires the instruments to be shut off. The particle background on the XIS detectors is produced by cosmic rays that penetrate the spacecraft shielding (Mizuno et al. 2004); it is generally lower for XIS than for ACIS and varies throughout the orbit as a function of the geomagnetic cutoff rigidity, a measure of how well the Earth's geomagnetic field shields the spacecraft from charged particles (Tawa et al. 2008).

2.3. Calibration Sources

Both ACIS and XIS have on-board radioactive ^{55}Fe sources used for instrument monitoring and calibration. The ACIS External Calibration Source (ECS) is mounted such that it is only viewable when ACIS is moved out of the focal plane. Observations of the ECS are done twice an orbit, just before and after perigee passages. The ECS provides roughly uniform illumination of the entire focal plane. Fluorescent Al and Ti targets provide lines at 1.5 keV (Al K) and 4.5 keV (Ti Kα), as well as those from the ^{55}Fe source itself at ~0.7 keV (Mn L), 5.9 keV (Mn Kα), and 6.4 keV (Mn Kβ).

The calibration sources on XIS illuminate the upper corners of each CCD during all observations. The spectral lines are from the ^{55}Fe source itself at 5.9 keV (Mn Kα), and 6.4 keV (Mn Kβ). The window of the source holder absorbs the low-energy Mn L lines. The orientation and approximate size of the regions illuminated by the calibration sources are shown in Figure 2.

The energy spectra of the ACIS and XIS calibration sources are shown in Figure 3. These data are from the BI CCDs taken early in each mission when performance was best. In the region around the Mn Kα line the spectra from the two sources look very similar to each other.

3. Methodology

3.1. Data and Analysis

The data used here have not gone through the standard pipeline processing that is normally applied to data distributed to users. Standard processing[1] is designed to remove some of the effects we are trying to study here, by applying corrections for CTI and time-dependent gain changes. The actual performance seen by a

[1] See http://cxc.harvard.edu/ciao/threads/data.html and http://heasarc.gsfc.nasa.gov/docs/suzaku/analysis/abc/

typical user from standard pipeline processed data is much improved from that reported here. These data have been minimally processed, by removing the CCD bias level and by applying a standard grade filter (ASCA G02346) and discarding all others. XIS1 and ACIS-S3 are used are representative BI CCDs and XIS3 and ACIS-I3 are representative FI CCDs.

As the XIS calibration sources only illuminate the upper corners of the CCDs, we filter the data to include only events within a rectangular region encompassing the calibration source events. The size of the region varies slightly between CCDs, but is roughly 225 pixels square. While the ACIS calibration sources fully illuminate the CCDs, the ACIS data were also filtered to roughly match the XIS regions.

The individual calibration source observations are then grouped together by time in bins of roughly a month. The ACIS data cover the time period from January 2000, when the focal plane temperature was initially lowered to its current value, to February 2011. The XIS data begin shortly after the *Suzaku* launch in July 2005 and continue through February 2011. The XIS data with and without charge injection are binned separately, as the performance is quite different.

The gain of the detector, the transformation from pulseheight to energy for each event, is determined by fitting a Gaussian to the pulseheight histogram in the initial time bin. The two corner regions must be fit separately, since they are in different readout nodes and do not have the same gain. This gain correction is then applied to all the time bins.

We then make an energy spectrum of the data in each time bin. Since we have already applied a gain correction, the two corner regions can be combined into one spectrum and fit together for better counting statistics. A Gaussian plus a linear background term is fit to the region around the Mn Kα line using Gehrels weighting (Gehrels 1986) which is a better approximation of the statistical error when the counts in the spectral bins can be small or zero. The Gaussian centroid and width are used in the subsequent sections of this paper to understand the evolution of CTI. Example spectra of the region around the Mn Kα line for the XIS FI CCD with and without charge injection are shown in Figure 4. Also shown are the best fit Gaussian plus background model.

3.2. A Proxy for Measuring CTI

A standard measurement of parallel CTI, or charge loss as a function of row, requires full illumination of the CCD with a source of known energy. The ECS on ACIS is capable of illuminating the entire CCD array with photons at a number of specific energies, as described in Section 2.3. The CTI on XIS is calibrated in a number of less direct ways, including a novel method of "checker flag" charge injection described further in Ozawa et al. (2009). Since the XIS calibration sources are incapable of illuminating the full chip, for proper comparison we must restrict our analysis to the upper corners of the ACIS chips as well. A change in CTI must change the accumulated charge loss and thus the pulseheight far from the framestore region. A change in pulseheight, however, does not necessarily have to be related to CTI in the imaging array; it could also be due to CTI changes in the framestore or changes in the gain completely unrelated to radiation damage. For example, ACIS has a known slow change in the gain as a function of time as measured very close to the framestore where imaging array CTI change should be negligible. For most of the CCDs it is monotonically decreasing at a rate of $\sim$ 2.4 eV or 0.04% per year at 5.9 keV.[2]

To determine the feasibility of using only the upper corners as a CTI metric, we compared the change in Mn Kα pulseheight to the measured CTI for two ACIS chips. The results are shown in Figure 5. Prior to correcting for the known gain change, the fractional pulseheight change is well-correlated to the CTI (left panels). After the correction, the correlation is even tighter (right panels). The correction coefficient was fit by eye, finding the value that best reduced the ACIS-I3 scatter. The correction is always less than 0.5% of the total pulseheight.

While the electronics of the two instruments are not identical, there's no reason to assume this should change the relationship of the line centroid to CTI. It is possible, however, that the harder spectrum of the particle radiation in low Earth orbit compared to Chandra's higher orbit could produce changes in the CTI of the framestore array. To further test this, we have examined multiple XIS observations of the Perseus cluster which is large enough to illuminate a substantial area of the CCDs and has been observed numerous times. The cluster spectrum has a strong iron line, which can be used, like the Mn Kα line in the calibration source, to directly measure the change in line energy as a function of row. We can then extrapolate this relation to find the line energy at row zero as a function of time. This value should be insensitive to increased radiation damage in the imaging array, and only dependent on changes in the framestore or changes in the electronic gain. Figure 6 shows this line energy change as a function of time. All the data shown were taken with charge injection active. The change in line energy independent of the imaging array CTI is 0.6% per year for XIS1 and 0.2% per year for XIS3. The difference between XIS1 and XIS3 may indicate that the cause for the line energy change is radiation damage in the framestore, rather than a gain change, which is being partially mitigated by the charge injection. The BI CCD charge injection is smaller than the FI CCD, so it receives less mitigation. If so, these can be considered lower limits for the line energy change in the framestore when charge injection is not active.

4. Discussion

4.1. CTI Time Evolution

We measure the time evolution of CTI using the change in line energy of the Mn Kα line, as described in the previous section. The change in line energy is plotted in Figure 7 (for XIS) and Figure 8 (for ACIS) as the fractional change since the first data point. Data from both front- and back-illuminated devices are included, as well as both with and without XIS charge injection.

Increasing CTI leads to decreasing measured line energy. All cases show an overall increase in CTI due to radiation damage. In some cases, the CTI increase from radiation damage is modified by sacrificial charge from the particle background, discussed further in Section 4.3. Charge injection also clearly modifies the rate of CTI increase. The rate of change of CTI varies substantially between the different cases.

4.1.1. Suzaku

The use of charge injection for the XIS greatly affects the inferred change in CTI. Charge injection was not used from the

[2] See http://space.mit.edu/home/cgrant/gain for example plots of the gain change.

beginning of the *Suzaku* mission through mid-2006; the rate of line energy change is roughly 2% per year during this time (see Figure 7). The FI and BI devices, while not identical, appear very similar. The line energy evolution appears to be approximately linear with time.

When charge injection is turned on, there are three notable changes. The first is that the line energy is restored to nearly its original value, since the charge injection produces significant sacrificial charge which improves the measured CTI. The second is that the rate of change of line energy is shallower than without charge injection. Finally, the improvement due to charge injection is larger for the FI CCD than for the BI device. The rate of line energy change is roughly 1.0% per year for the BI CCD and 0.4% per year for the FI CCD. After removing the gain change measured in Section 3.2, the rate of line energy change is roughly 0.4% per year for the BI CCD and 0.2% per year for the FI CCD.

The FI/BI difference is due to the fact that the amount of charge injected is higher for the FI CCD than for the BI CCD (Bautz et al. 2007). In particular, for the FI CCD the injected charge level is higher than the X-ray line energy of the calibration source and for the BI CCD is much lower than the line energy. The amount of charge injection on the BI CCD is insufficient to provide the full potential mitigation. It should be noted that the amount of injected charge on the BI CCD was increased in mid-2011 and since that time the rate of line energy change of the BI CCD is nearly the same as the FI CCD (LaMarr et al. 2012). We have not included the recent data in this analysis.

4.1.2. Chandra

The change in line energy for ACIS is very different from XIS, as can be seen in Figure 8. ACIS does not have the capability to inject a known quantity of charge like XIS, so the only sacrificial charge is from the particle background and the X-ray photons themselves. The rate of line energy change is much lower for ACIS than it is for XIS. Assuming a linear decay, the change is roughly 0.12% per year for the BI CCD and 0.10% per year for the FI CCD. After removing the known gain change discussed in Section 3.2, the change in ACIS line energy is roughly 0.08% per year for the BI CCD and 0.05% for the FI CCD.

The evolution of the FI and BI CCDs look quite different as well. The FI CCDs appear to be much more sensitive to sacrificial charge from the particle background than the BI CCDs. The decrease is clearly not strictly linear, due to the changing sacrificial charge which adds both features from individual solar storms and a larger modification tied to the solar cycle. This is seen in distinct features common to the plots of line energy and particle backgrounds as a function of time; periods of low background correspond to periods of increased CTI, and vice versa (see Figure 9). This FI/BI distinction cannot be due to differences in the number and type of particles impinging on the CCDs because they are in the same orbital environment, but must result from how the particles interact with the CCD structure. Sacrificial charge from the changing particle background and the FI/BI difference will be discussed further in Section 4.3.

4.2. Spectral Resolution Time Evolution

The spectral resolution is measured as the FWHM of the Mn Kα line. The time evolution of spectral resolution is shown in Figures 10 and 11 for XIS and ACIS, respectively. Data from both front- and back-illuminated devices are included, as well as both with and without XIS charge injection.

The relationship between increasing CTI and spectral resolution is not as simple as that for line energy. If an X-ray event occupies a single pixel, the charge loss due to CTI essentially adds an additional noise term to the spectral resolution. In the case of both ACIS and XIS, many events are split over multiple pixels. In that case, charge loss adds additional noise terms from all of the split pixels. In addition, some of the lost charge may be re-emitted into a trailing pixel which may also be included in the event depending on the size of the trailing charge. The combined effects of these processes result in a broader FWHM than would be measured in the absence of CTI.

4.2.1. Suzaku

The spectral resolution of the XIS devices shows temporal effects from both CTI and operational changes (see Figure 10). Initially, before charge injection was turned on, the rate of increase of spectral resolution for FI and BI CCDs was very similar, about 50 eV per year. Once charge injection was turned on, the performance improved and FWHM dropped to nearly the initial value. The rate of increase is much slower with charge injection than without, although again, the FI CCD shows more improvement than the BI CCD due to the larger amount of injected charge in the FI devices. The FWHM increase is about 9 eV per year for the FI CCD and about 13 eV per year for the BI CCD. As discussed in Section 4.1.1, after the increase in the amount of injected charge on the BI CCD in mid-2011, the FI and BI CCDs have nearly the same rate of FWHM change.

4.2.2. Chandra

The spectral resolution time dependence for ACIS differs from that of XIS (see Figure 11). The initial FWHM for both ACIS devices is much higher than that for XIS. This is due to the prelaunch manufacturing defects on the BI CCD (see Section 2.1) and the initial radiation damage to the FI CCDs in 1999 (see Section 2.2), before the time period shown here. The rate of increase, however, is vanishingly small, less than 1 eV per year for the BI CCD and consistent with no change for the FI CCD. Unlike the line energy, the FWHM evolution shows no obvious dependence on the particle background.

4.3. CTI and Spectral Resolution: Dependence on Background

As stated previously, measured CTI is a function of the amount of charge deposited on the CCD. Increasing the amount of sacrificial charge improves performance and lowers CTI. Figure 12 shows images of typical raw CCD frames for both ACIS and XIS and both types of CCDs. Essentially all the visible features are due to cosmic ray charged particles. While the images do include X-ray events from the calibration sources and (in the case of XIS) celestial sources, they are nearly invisible due to their small size and low numbers. In the absence of controlled charge injection, as is now routine on Suzaku, the most important source of sacrificial charge is from particle interactions.

The most obvious distinction is that between the FI and BI CCDs due to their structural differences. The FI CCDs display large streaks and blobs while the BI CCDs have much smaller features. The FI CCDs have an active, depleted region and a much thicker field-free region in the silicon substrate. The X-ray events generally interact in the depleted region so the charge is collected in a small area. Charged particles can traverse the en-

tire thickness of the CCD, depositing charge along their path. The charge in the field-free region can disperse more freely and produces the large blobs seen in the image. The BI CCDs are fully depleted, without the additional field-free region. The charge from particles stays more concentrated into smaller blobs and streaks. Comparing the FI and BI images from a single instrument, such as ACIS, shows that the total number of particle hits is comparable even though their morphology is so different.

The number of particle events is different between XIS and ACIS. ACIS clearly shows more particle events than XIS, even though the ACIS frame exposure time, 3.2 sec, is less than half that of XIS, 8 sec. This is due to the particle environment in the two orbits. Suzaku is in a low-earth orbit and receives substantial shielding from the Earth's magnetic field while Chandra's orbit takes it well above the magnetosphere and does not receive the same shielding.

This can also be seen in Figure 13 which shows the particle backround spectrum from each instrument after event recognition and filtering. The ACIS data was taken while the instrument was stowed and not under its calibration source, while the XIS data was taken looking at the dark Earth. In both cases, the only X-rays are due to materials fluorescing in the instrument with the remainder of the events from particle interactions. Both XIS CCDs have much lower particle background levels than ACIS, due to the different orbits. The BI devices have higher levels than the FI devices, as the larger cosmic ray blooms seen on the FI CCDs are more efficiently filtered out of the event list.

One might assume that the higher particle rate on the ACIS raw frames would translate to faster accumulation of radiation damage, but that is not necessarily the case. One reason is that the raw frames and the particle spectra represent only a snapshot of the relative particle rates at a particular time. Both orbits intersect regions with much higher particle rates (Earth's radiation belts and the SAA) that will not be seen in the data as the instruments are shut down. The total radiation dosage needs to consider the environment during the entire orbit and during times of high solar activity, not just while data is being collected. A second reason is that the measured CTI (Figures 7 and 8) is a function not only of the accumulated radiation damage, but also the sacrificial charge and the focal plane temperatures (see Section 4.4).

These basic distinctions in the number and morphology of particle events can explain some of the differences between the CTI evolution of ACIS and XIS. An additional piece of the puzzle is the time-dependence of the particle events themselves. Figure 9 shows a measure of the ACIS particle background over the same time period and with the same binning as the line energy evolution data. In this case the rate of high energy events rejected on-board the spacecraft is used as a proxy for the particle rate. These events are well above the X-ray energies that can be focused by the telescope and can only be caused by particles. The particle background rate is clearly not constant but is lowest in 2001 and reaches more than twice that level in 2010. It has been shown that this measure of the ACIS particle background is well correlated over long time-scales with proton fluxes measured by the Advanced Composition Explorer (Stone et al. 1998) spacecraft with energies above 10 MeV (Grant et al. 2002). The lower particle fluxes are due to extra shielding provided by the solar magnetic field during solar maximum. Additional smaller scale dips can be seen which can be directly linked to increased heliomagnetic shielding during specific solar storms. The solar storms also produce transient increases in the particle background, but these are over much shorter timescales, hours to days, and thus do not appear in Figure 9.

We can use these dips in the line energy to quantify the strength of its dependence on sacrificial charge from the particle background. A correction for sacrificial charge is part of the ACIS instrument team's standard CTI monitoring program described in Grant et al. (2005), although the correction factors have evolved since then. We can apply these correction factors to our line energy data to get a better sense for the true CTI change in the absence of sacrificial charge from the particle background. This corrected line energy and the line energy with no correction are shown in Figure 14. The CTI evolution is now much smoother, with a slightly higher rate of increase during solar maximum (2000–2002). After removing the gain change discussed in Section 3.2 and assuming a linear dependence, the rate of change is now 0.08% and 0.18% per year for the BI and FI CCDs, respectively, as compared to the background-uncorrected values of 0.08% and 0.05% per year.

Due to the shielding from the Earth's magnetic field, the long-term variability of the XIS particle background is very small. Tawa et al. (2008) found that after removing the orbital modulation and with the exception of a brief period of high solar activity, the particle background on XIS was constant within ±6% per year. **Eric is working on an update with longer time scale since Tawa's is only six months.**

A much stronger variability is induced by the Earth's geomagnetic field as the spacecraft travels about its ~96-minute orbit. Geomagnetic cut-off rigidity (COR) quantifies the shielding provided by the geomagnetic field at a particular orbital position. High values of COR correspond to regions with higher shielding and therefore lower particle background. In particular, we are using the quantity COR2, as defined in Tawa et al. (2008). The count rate of the particle background more than doubles between the highest and lowest COR values (Tawa et al. 2008). **looking back at Tawa, it's closer to 3x than 2x** The dependence of line energy on cut-off rigidity is shown in Figure 15. In general, line energy is only weakly dependent on cut-off rigidity, and that dependence disappears when charge injection is active. In the absence of charge injection, the line energy varies by about 0.2% over the entire range of COR values for both the BI and FI CCDs, with slightly higher line energies at low COR, as is expected for sacrificial charge from the particle background. With charge injection, this minimal dependence disappears, as the injected charge completes overwhelms the charge from the particle background.

The ACIS FI CCD line energy appears to have a much stronger dependence on sacrificial charge from the particle background than the ACIS BI CCD or XIS. Over the entire range of ACIS particle background rates, about a factor of two, the line energy changes by about 1.5% for the FI CCD and about 0.01% for the BI CCD. Without charge injection, the XIS line energy changes by only about 0.2% over the entire range of COR values, which is also about a factor of two in particle rates. The absolute level of the particle background is much higher for ACIS than for XIS. For example, in the typical raw images shown in Figure 12, the total charge per frame from both particles and X-rays is more than two times higher for ACIS than for XIS. While this does make sacrificial charge more important for ACIS than XIS, the two ACIS CCD types are seeing the same particle flux and yet have different sacrificial charge dependencies. **need a reference to papers with time constants or talk about trailing charge here.**

In contrast to the line energy evolution, the line width for ACIS does not appear to have any dependence on sacrificial charge. None of the strong features seen in the line energy and particle background (Figure 9) are seen in Figure 11. The XIS

line width, however, does show a weak dependence on cut-off-rigidity in the absence of charge injection and varies by about 15 eV over the entire range of COR values (Figure 16). **need more here. refer back to section 4.2, make revelant to sacrificial charge.**

4.4. CTI and Spectral Resolution: Dependence on Temperature

At least some of the differences between the evolution of CTI on ACIS and XIS can possibly be due to operating at different focal plane temperatures. ACIS is kept much colder at −120°C than XIS at −90°C, so many of the common electron traps that cause CTI have been frozen out. In order to minimize the effect of the sacrificial charge from the particle background, we can compare the line energy evolution of ACIS after the sacrificial charge correction discussed in the previous section (Figure 14) to XIS without charge injection (Figure 7). The rate of change is much higher for XIS than for ACIS by about an order of magnitude for both the FI and BI CCDs. While this could be due to a higher level of damaging particle radiation, it could also be due to the higher CCD temperatures. **this comparison isn't completely fair yet – I'm removing the gain decrease for ACIS which reduces the final CTI change number, but I'm not doing anything equivalent for XIS**

Fortunately, the ACIS team has performed a series of CTI measurements at different temperatures on two occasions separated by six years (Grant et al. 2006). We can use this data to compare the time evolution at −120°C and −90°C, determine how large the CTI change on ACIS would be at either temperature, and then compare to the actual change measured for XIS to see how much of the difference is due to temperature rather than anything else. We have reanalyzed the data used in Grant et al. (2006) to duplicate the data analysis techniques used in this paper. The representative FI CCD, ACIS-I3, was not in use during the first set of temperature measurements, so it is replaced in this analysis by ACIS-S2 which should have similar characteristics. We can only compare the line energy and not the line width evolution, as the much higher level of CTI on ACIS makes measurement of the width at warm temperatures problematic. For both the FI and BI CCDs, the change in line energy with time is about three times larger at −90°C than at −120°C which can be compared to the order of magnitude difference in the previous paragraph. While temperature can explain some of the difference between the line energy evolution of ACIS and XIS, it cannot account for all of the difference.

5. Conclusions

Conclusions TBD. Summarize what we've said so far, try to make it make sense.

Line evolution.

- XIS no CI, strong time evolution, weak particle background dependence
- XIS with CI, slower time evolution, no particle background dependence
- ACIS, even slower time evolution, strong particle background dependence (FI more than BI)
- XIS no CI, 1.87%/yr (BI), 2.01%/yr (no sac. charge correction necessary; low, non-varying particle background)
- XIS no CI, "gain" corrected, TBD
- XIS with CI, 0.99%/yr (BI), 0.38%/yr (FI)
- (BI with new CI is ∼same as FI)
- XIS with CI, "gain" corrected, 0.39%/yr (BI), 0.18%/yr (FI)
- ACIS sac. charge removed, 0.08%/yr (BI), 0.18%/yr (FI) (gain corrected)
- ACIS sac. charge removed, corrected to -90C, 0.22%/yr (BI), 0.46%/yr (FI).
- Still smaller than XIS no CI. => XIS dosage is larger?
- XIS FI/BI line energy change about the same, ACIS FI/BI not the same. => ACIS getting more soft particles than XIS.

Spectral resolution. (This is harder, working on the logic)

Acknowledgements. The authors thank blah blah and blah blah for such and such. This work was supported by NASA contracts NAS 8-37716, NAS 8-38252, and NNX-09AE58G, and by funding from the Institute of Space and Astronautical Science, Japan Aerospace Exploration Agency. **need to check the Suzaku funding stuff, stolen from old Bev paper. Also I think this is the old ACIS GTO grant.**

References

Bautz, M. W., Kissel, S. E., Prigozhin, G. Y., et al. 2004, in Society of Photo-Optical Instrumentation Engineers (SPIE) Conference Series, Vol. 5501, Society of Photo-Optical Instrumentation Engineers (SPIE) Conference Series, ed. A. D. Holland, 111–122

Bautz, M. W., LaMarr, B. J., Miller, E. D., et al. 2007, in Society of Photo-Optical Instrumentation Engineers (SPIE) Conference Series, Vol. 6686, Society of Photo-Optical Instrumentation Engineers (SPIE) Conference Series

Burke, B. E., Gregory, J. A., Loomis, A. H., et al. 2004, IEEE Transactions on Nuclear Science, 51, 2322

Garmire, G. P., Bautz, M. W., Ford, P. G., Nousek, J. A., & Ricker, Jr., G. R. 2003, in Society of Photo-Optical Instrumentation Engineers (SPIE) Conference Series, Vol. 4851, Society of Photo-Optical Instrumentation Engineers (SPIE) Conference Series, ed. J. E. Truemper & H. D. Tananbaum, 28–44

Gehrels, N. 1986, ApJ, 303, 336

Gendreau, K., Bautz, M., & Ricker, G. 1993, Nuclear Instruments and Methods in Physics Research A, 335, 318

Grant, C. E., Bautz, M. W., Kissel, S. E., LaMarr, B., & Prigozhin, G. Y. 2006, in Society of Photo-Optical Instrumentation Engineers (SPIE) Conference Series, Vol. 6276, Society of Photo-Optical Instrumentation Engineers (SPIE) Conference Series

Grant, C. E., Bautz, M. W., Kissel, S. M., LaMarr, B., & Prigozhin, G. Y. 2005, in Society of Photo-Optical Instrumentation Engineers (SPIE) Conference Series, Vol. 5898, Society of Photo-Optical Instrumentation Engineers (SPIE) Conference Series, ed. O. H. W. Siegmund, 201–211

Grant, C. E., Bautz, M. W., & Virani, S. N. 2002, in Astronomical Society of the Pacific Conference Series, Vol. 262, The High Energy Universe at Sharp Focus: Chandra Science, ed. E. M. Schlegel & S. D. Vrtilek, 401

Koyama, K., Tsunemi, H., Dotani, T., et al. 2007, PASJ, 59, 23

LaMarr, B. J., Bautz, M. W., Kissel, S. E., Miller, E. D., & Prigozhin, G. Y. 2012, in Society of Photo-Optical Instrumentation Engineers (SPIE) Conference Series, Vol. 8443, Society of Photo-Optical Instrumentation Engineers (SPIE) Conference Series

Mitsuda, K., Bautz, M., Inoue, H., et al. 2007, PASJ, 59, 1

Mizuno, T., Kamae, T., Godfrey, G., et al. 2004, ApJ, 614, 1113

O'Dell, S. L., Bautz, M. W., Blackwell, W. C., et al. 2000, in Society of Photo-Optical Instrumentation Engineers (SPIE) Conference Series, Vol. 4140, Society of Photo-Optical Instrumentation Engineers (SPIE) Conference Series, ed. K. A. Flanagan & O. H. Siegmund, 99–110

Ozawa, M., Uchiyama, H., Matsumoto, H., et al. 2009, PASJ, 61, 1

Prigozhin, G. Y., Kissel, S. E., Bautz, M. W., et al. 2000, in Society of Photo-Optical Instrumentation Engineers (SPIE) Conference Series, Vol. 4140, Society of Photo-Optical Instrumentation Engineers (SPIE) Conference Series, ed. K. A. Flanagan & O. H. Siegmund, 123–134

Stone, E. C., Frandsen, A. M., Mewaldt, R. A., et al. 1998, Space Sci. Rev., 86, 1

Tawa, N., Hayashida, K., Nagai, M., et al. 2008, PASJ, 60, 11

Uchiyama, H., Ozawa, M., Matsumoto, H., et al. 2009, PASJ, 61, 9

Weisskopf, M. C., Brinkman, B., Canizares, C., et al. 2002, PASP, 114, 1

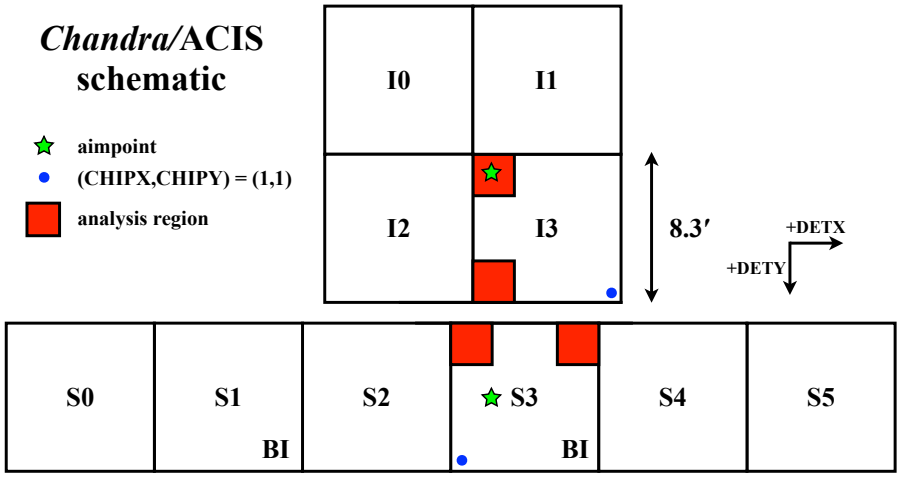

Fig. 1. Schematic drawing of the ACIS focal plane. The orange squares indicate the regions used for data analysis in this paper. The green stars show the standard aimpoints on ACIS-I3 and ACIS-S3.

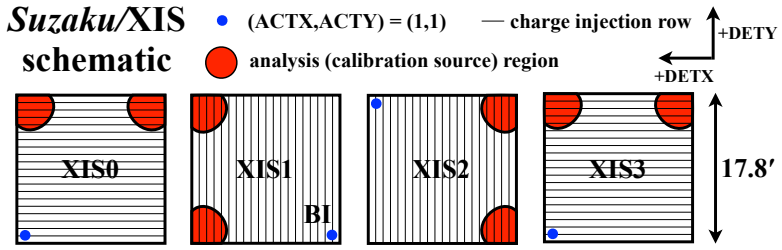

Fig. 2. Schematic drawing of the XIS focal plane. The orange circles show the regions illuminated by the ^{55}Fe sources. The light grey lines indicate the direction and spacing of the charge injection rows.

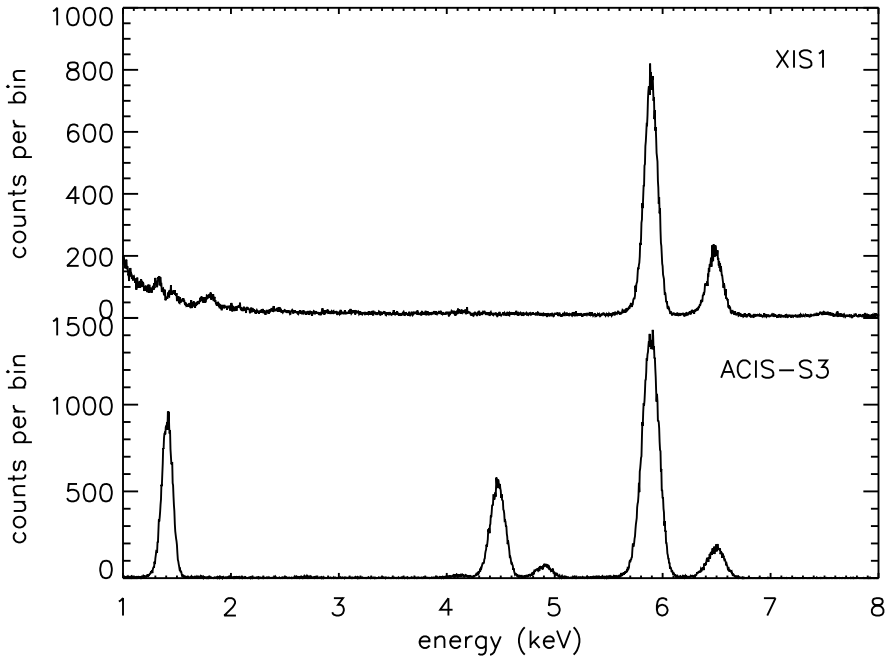

Fig. 3. Example spectra of the XIS and ACIS calibration sources using the BI CCDs taken early in each of the missions when performance was best. Both sources have strong Mn Kα and Mn Kβ lines around 6 keV. The ACIS source has additional lines from Titanium and Aluminum.

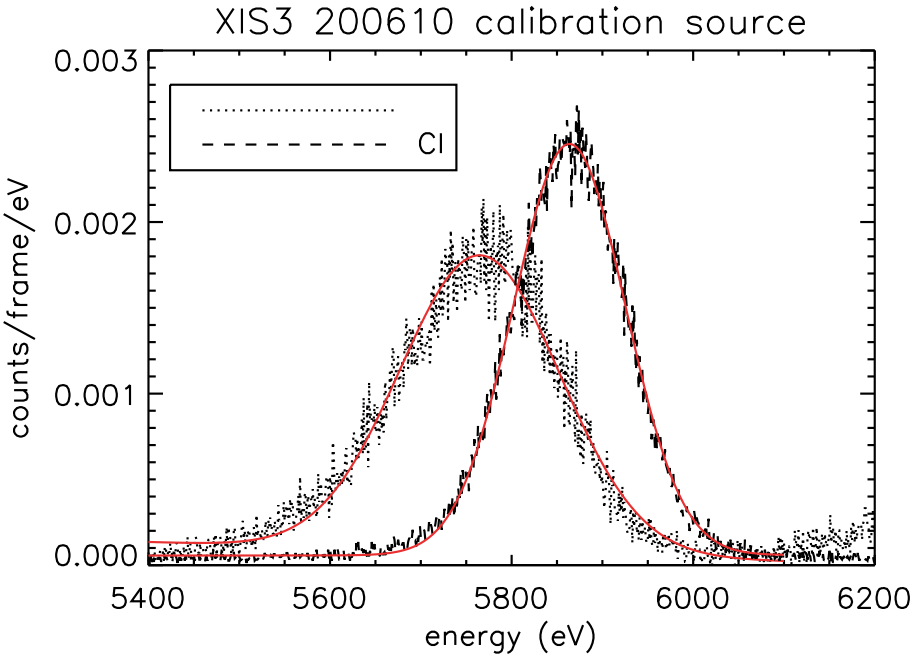

Fig. 4. Spectrum of the Mn Kα line at 5.9 keV for the XIS FI CCD. Without charge injection (dotted line), the line is broader and shifted to lower energies. Charge injection (dashed line) improves both the line centroid and the width. The red line is the best fit Gaussian plus linear background.

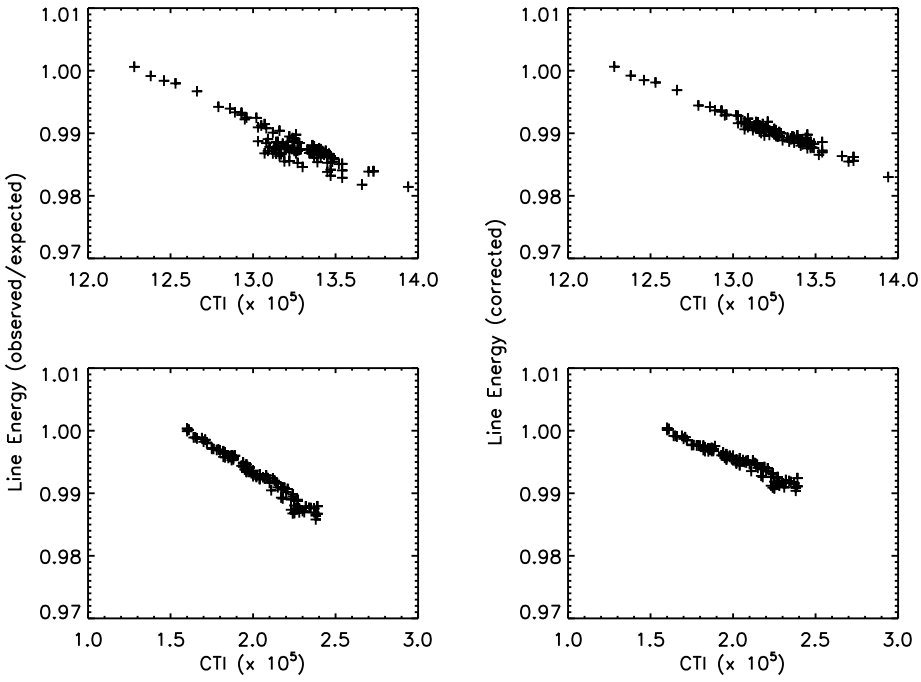

Fig. 5. CTI ($\times 10^5$) versus the fractional change in Mn Kα line energy for two ACIS devices, the FI CCD I3 (top) and the BI CCD S3 (bottom), as measured from the upper corners of each chip. The left panels show the measured data, while the right panels show data corrected for a slow gain decrease, discussed in the text. The CTI and pulseheight are well-correlated.

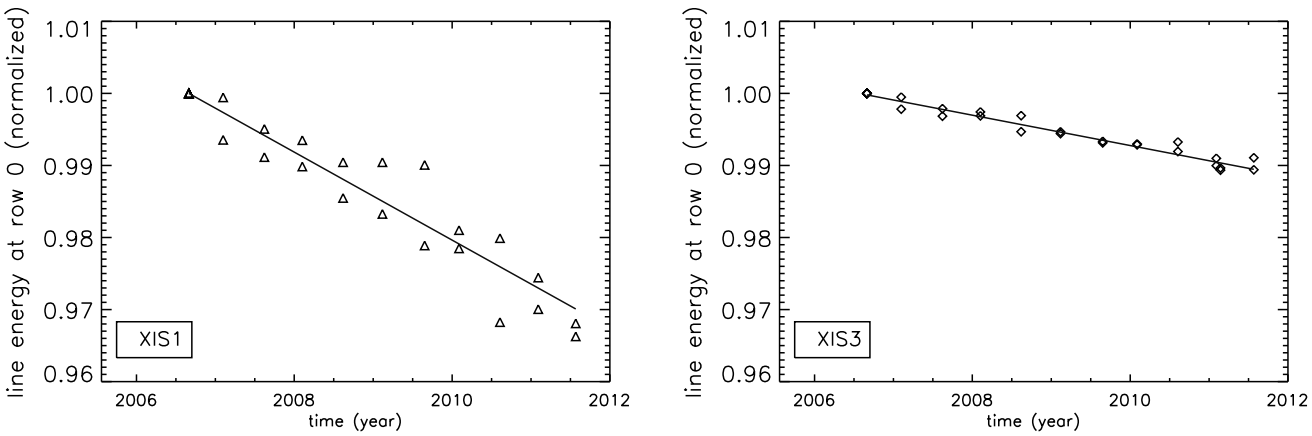

Fig. 6. Fractional change in the XIS line energy at the bottom of the imaging array, measured using the iron line in observations of the Perseus cluster. Each observations has two data points, one from each of the two central quadrants of the CCD.

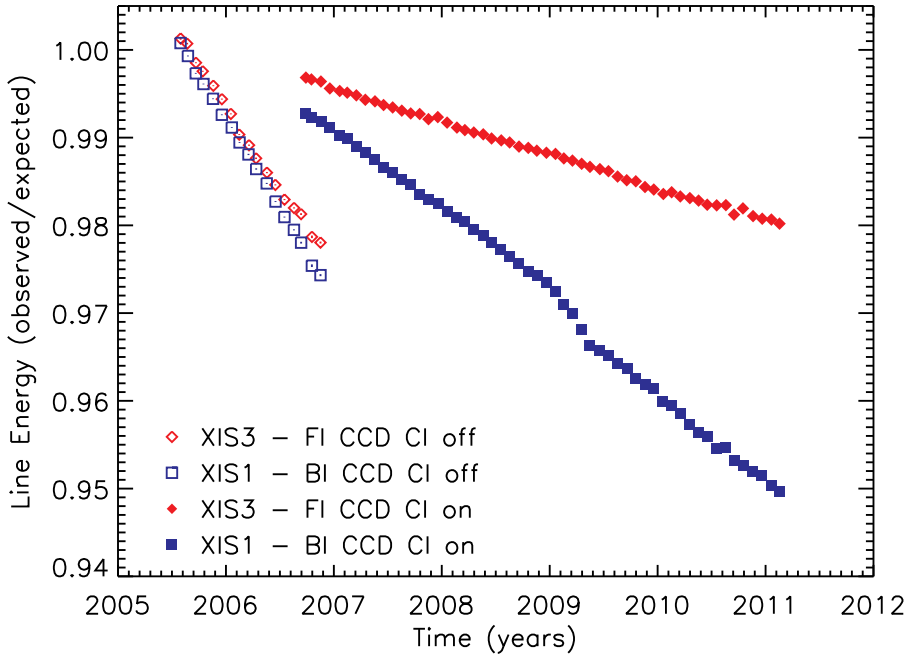

Fig. 7. Fractional change in the XIS line energy over the course of the *Suzaku* mission, as measured at Mn Kα. Different symbols show FI and BI devices with charge injection (CI) on and off. The 1-σ error bars are shown but are much smaller than the symbol sizes.

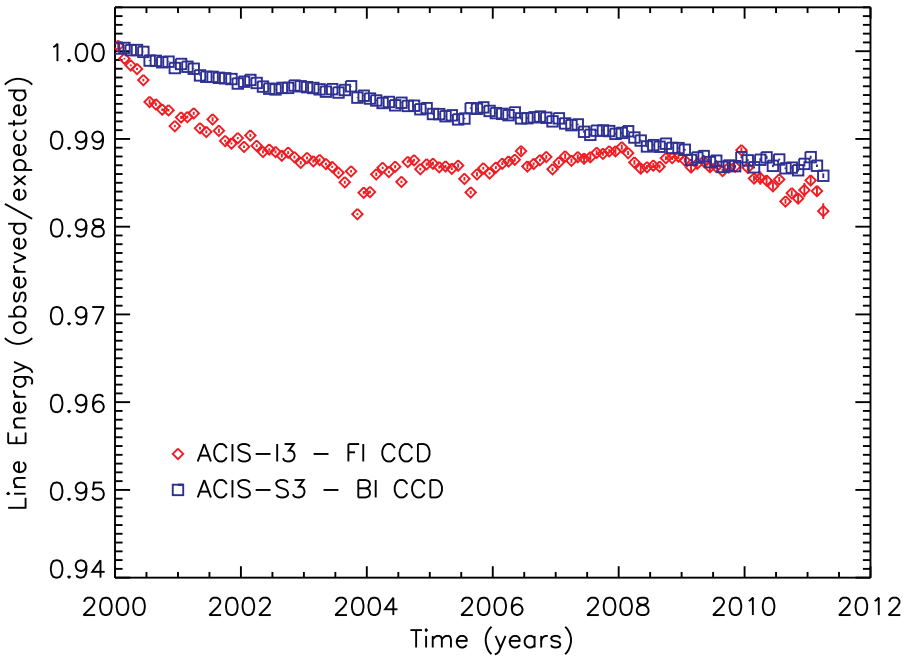

Fig. 8. Fractional change in ACIS line energy over the course of the *Chandra* mission, as measured at Mn Kα. The effects of varying particle background and sacrifical charge are seen in the ACIS-I3 (FI) data. The 1-σ error bars are shown but are often smaller than the symbol sizes.

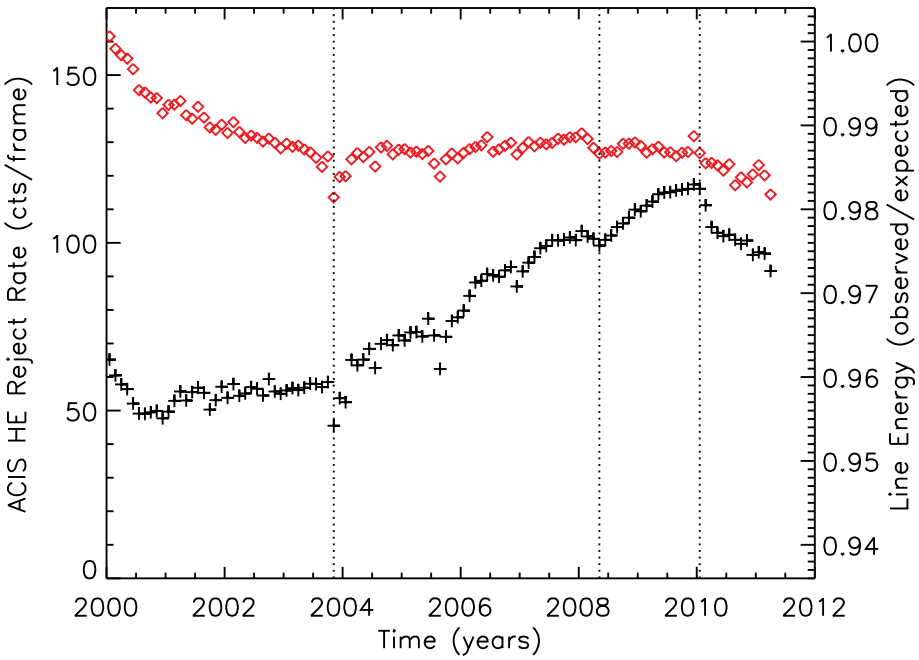

Fig. 9. Time history of the particle background of the *Chandra* mission, measured as the rate of high energy events on ACIS-S3 (BI), shown as black crosses. The time period and binning are the same as the CTI evolution data. The structure from the varying particle background can been seen in the ACIS FI CCD line energy data, shown in red. The vertical lines demonstrate the simultaneous nature of the structures.

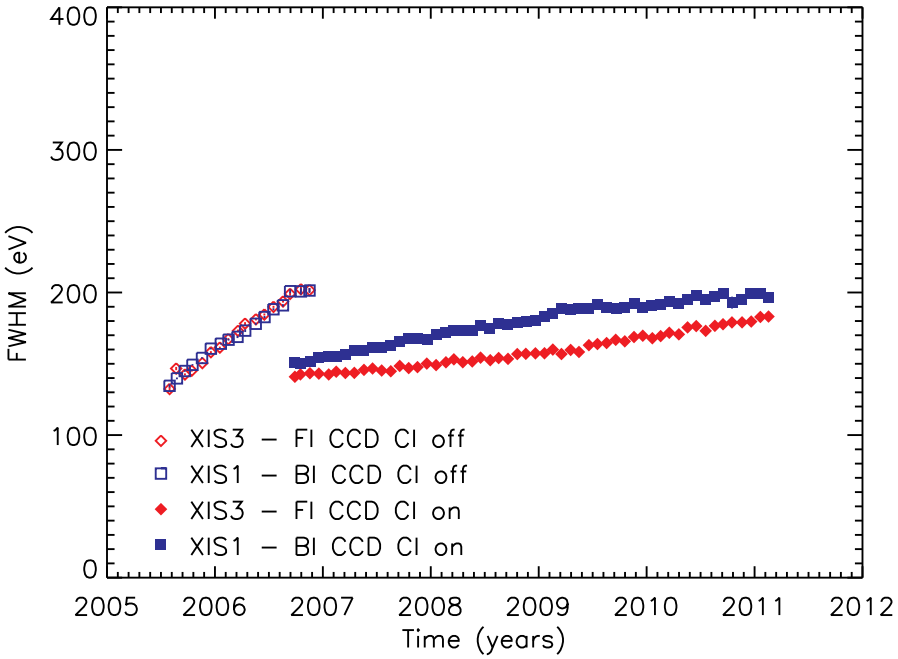

Fig. 10. Change in XIS line width (FWHM) with time over the course of the *Suzaku* mission, as measured at Mn Kα. Different symbols show FI and BI devices with charge injection (CI) on and off. The 1-σ error bars are shown but are often smaller than the symbol sizes.

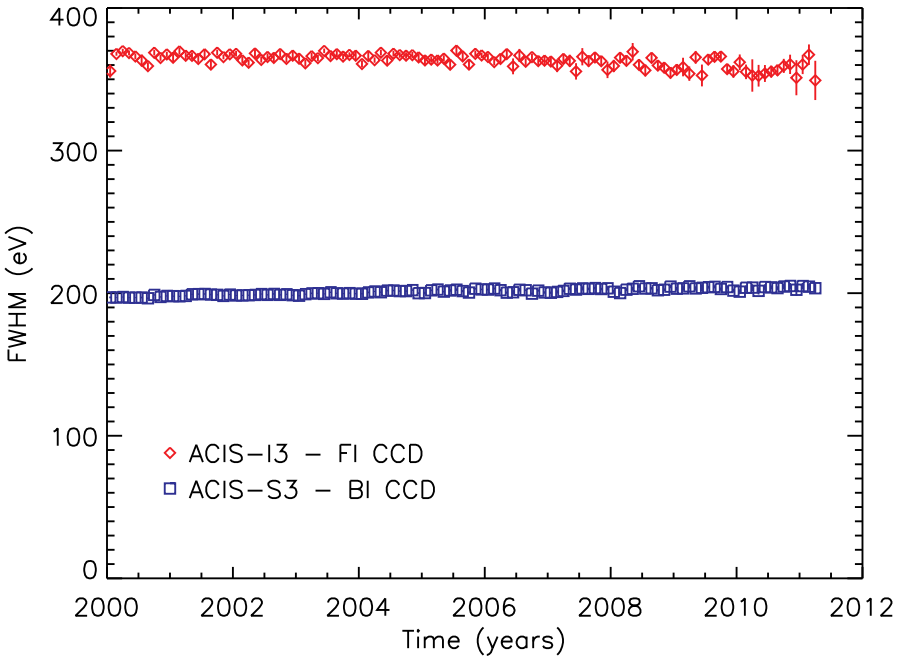

Fig. 11. Change in ACIS line width over the course of the *Chandra* mission, as measured at Mn Kα. The 1-σ error bars are shown but are often smaller than the symbol sizes.

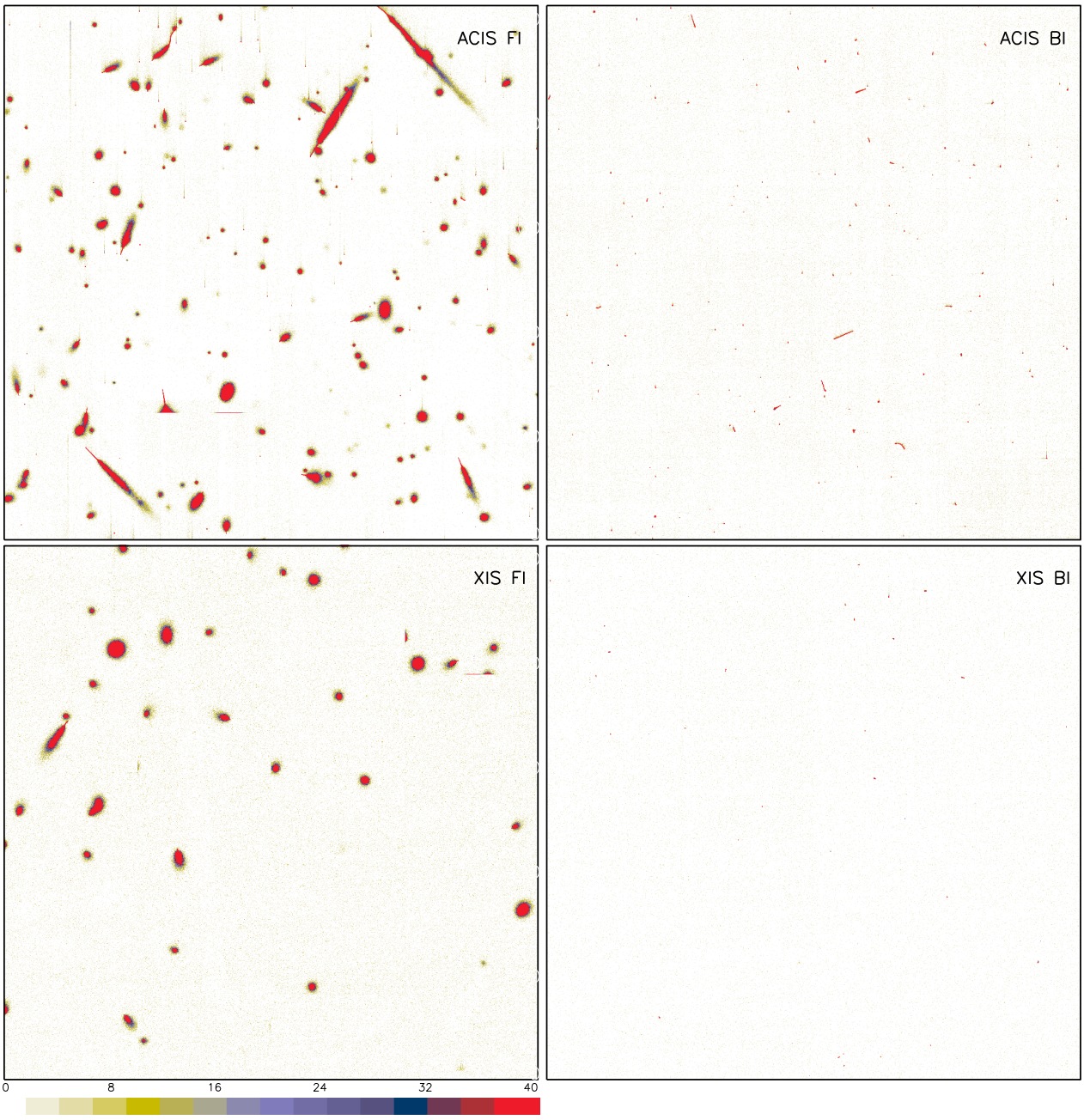

Fig. 12. Typical raw frame images for ACIS (top) and XIS (bottom), showing an FI (left) and BI (right) device for each. The colorbar shows the pixel values in ADU. An X-ray event from ^{55}Fe would have a pulseheight around 1500 ADU. The differences between the FI and BI CCDs, and between ACIS and XIS are explained in the text.

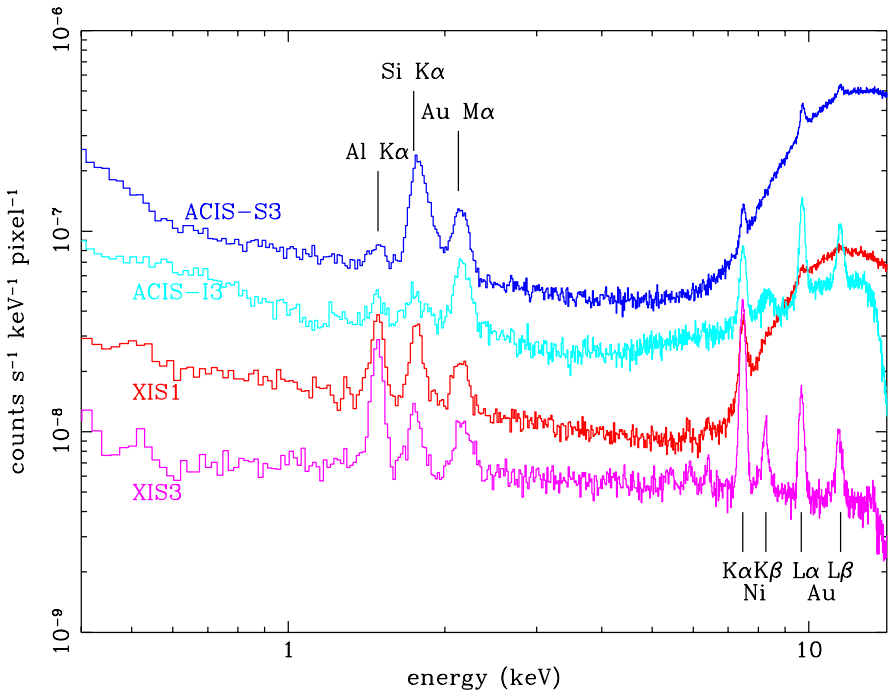

Fig. 13. Spectrum of the particle background seen by ACIS and XIS after standard event detection and filtering. The rate of particle events is higher for ACIS compared to XIS due to the different orbits. The BI CCDs have a higher rate of particle events than the FI CCDs, due to their structural differences. The larger blooms produced by particles on the FI CCD are more efficiently filtered in the event selection process than on the BI CCD.

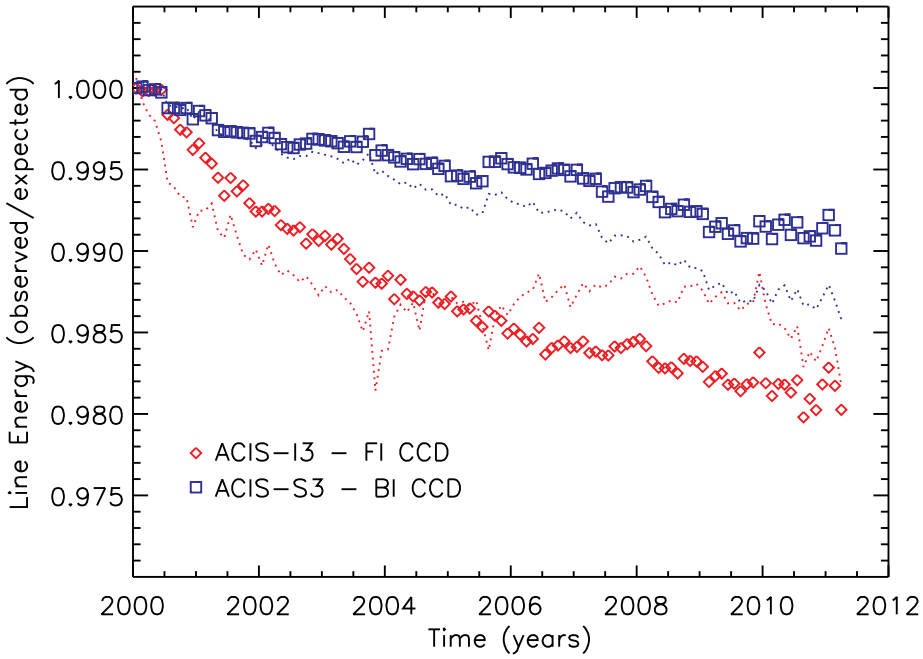

Fig. 14. Fractional change in ACIS line central energy over the course of the *Chandra* mission, after correcting for sacrificial charge from the particle background. For comparison, the dotted lines show the uncorrected line energy as in Figure 8.

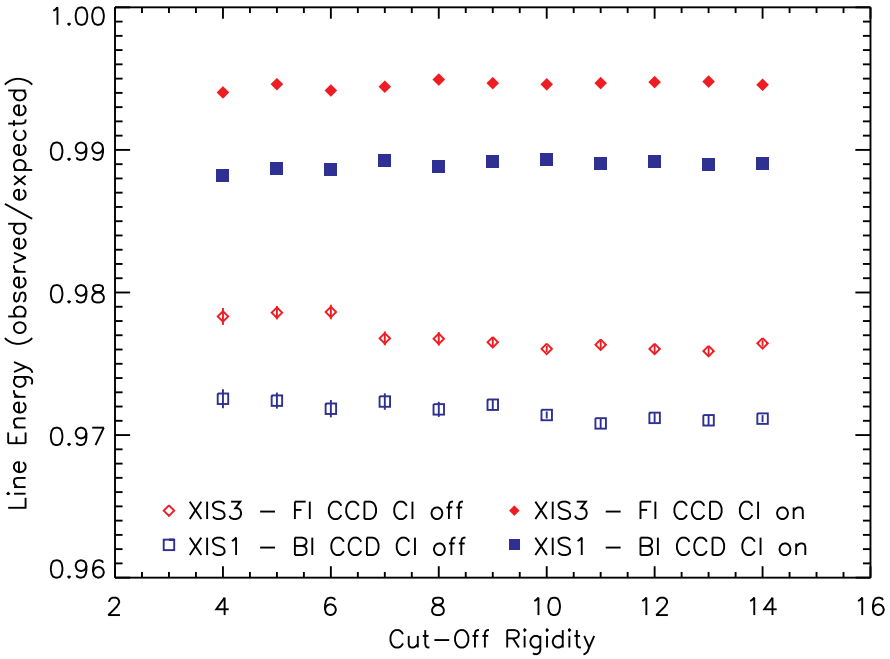

Fig. 15. Fractional change in the XIS line energy as a function of geomagnetic cut-off rigidity (COR), averaging over October-November 2006. Symbols are the same as in Figure 7. Without charge injection, there is a weak dependence of line energy with COR, with higher line energy associated with lower COR, as is expected for sacrificial charge. The use of charge injection overwhelms the effects of sacrificial charge from the particle background (solid symbols). The 1-σ error bars are shown but are often smaller than the symbol sizes.

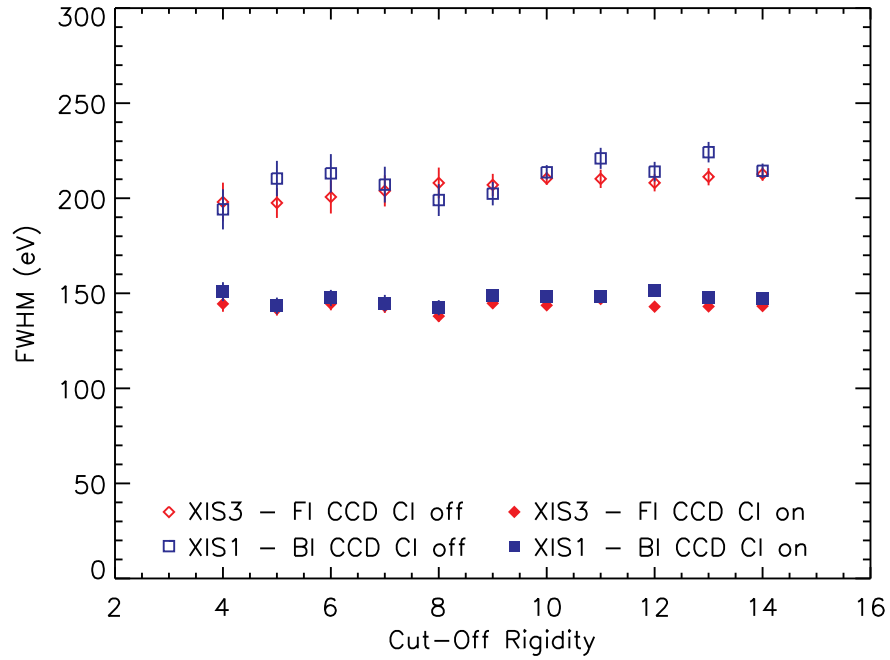

Fig. 16. XIS Mn Kα line width (FWHM) as a function of COR, averaging over October-November 2006. Symbols are the same as in Figure 10. Lower cut-off rigidity indicates a higher particle background, therefore the narrower line widths at low COR in the absence of charge injection (open symbols) are due to sacrificial charge. Use of charge injection overwhelms the effects of sacrificial charge, so no dependence on COR is seen in those data (solid symbols).

Table 1. Characteristics of MIT Lincoln Laboratory CCDs for ACIS and XIS

	ACIS	XIS
Model	CCID17	CCID41
Format	1026 rows × 1024 pixels/row (imaging area)	
Architecture	3-phase, frame-transfer, four parallel output nodes	
Illumination Geometry	8 FI & 2 BI	2 FI & 1 BI
Charge Injection Capable	no	yes
Pixel Size	$24 \times 24 \mu$m	
Readout Noise (RMS)	2–3 e^- at 400 kpix s^{-1}	< 2.5 e^- at 41 kpix s^{-1}
Depletion Depth	FI: 64–76 μm; BI: 30–40 μm	FI: 60–65 μm; BI: 40–45 μm
Operating Temperature	−120°C via radiative cooling	−90°C via Peltier cooler
Frame Transfer Time (per row)	40 μs	24 μs
Frame Exposure Time[a]	3.2 s	8.0 s
Pre-Launch CTI (10^{-5})	FI: < 0.3	FI: 0.3–0.5
	BI: 1–3	BI: 0.55

[a] In normal operating mode.